In Vivo MRI and X-Ray Bifunctional Imaging of Polymeric Composite Supplemented with $GdPO_4 \cdot H_2O$ Nanobundles for Tracing Bone Implant and Bone Regeneration

Jing Huang, Zhongwen Lv, Yu Wang, Zongliang Wang, Tianlin Gao, Ning Zhang, Min Guo, Haifeng Zou, and Peibiao Zhang**

A multifunctional hybrid system which combines two or more functions to form nanobiological and nanomedical platforms has gained more and more attention.[1] Most of them are candidates to be employed for various biomedical applications in drug tracing and cancer therapies. However, there are few reports on their application in polymeric bone implants for X-ray or magnetic resonance (MR) imaging.

Poly(lactic-co-glycolic acid) (PLGA) is a biodegradable copolymer composed of lactic acid and glycolic acid and its degradation rate can be adjusted according to the ratio of the two monomers. They have good biocompatibility and good performance for fabrication of capsules, films, and scaffolds, and are widely used in pharmaceutical and tissue engineering as a FDA certificated medical materials.[2] On the other hand, hydroxyapatite (HA) is the main component of bone tissue in the human body. Synthesized HA nanoparticles are chemically and structurally similar to the native ones, and exhibit improved biodegradability and biological activity compared to HA ceramics thanks to their nanosize dimensions and large specific surface areas. After implanted, calcium and phosphorus can be freed to the surface, absorbed by the body, and grow into a new organization.[3] In general, they are usually used as a component of nanocomposites incorporated with natural or synthetical biodegradable polymers for bone tissue engineering or fixing devices including, but not limited to, collagen, chitosan, poly(L-lactide) (PLA), and PLGA.[4,5]

Recently, more and more studies on HA and PLGA nanocomposites for biodegradable bone implants are reported.[6,7] However, their application in vivo is limited mainly because the modifications of the implants cannot be clearly monitored using conventional X-ray image diagnosis or magnetic resonance imaging (MRI) after implantation.

Rare earth materials have excellent optical, electric, and magnetic properties because of the 4f electronic configuration. Lanthanide phosphates have several advantages such as low toxicity, good chemical durability, and thermal stability. In addition to being luminescent material matrix, gadolinium (Gd)-based nanoparticles (Gd_2O_3, Gd_2O_2S, $GdPO_4 \cdot nH_2O$, and $NaGdF_4$) can be used as MRI contrast agents due to their unpaired 4f electrons. Most of them were used for controlling drug delivery or oncotherapy and few of them were applied in tracing bone fixing devices or bone scaffolds in vivo.[8,9] Furthermore, some studies have shown that phosphate is a signal molecule in osteoblast differentiation.[10,11] Thus, nanomaterials containing Gd^{3+} and PO_4^{3-} may represent good candidates for solving the problem of in vivo tracing of polymeric bone-substitute materials.

In this study, homogeneous and monodisperse $GdPO_4 \cdot H_2O$ nanobundles have been successfully synthesized via a solvothermal method. Then, the nanobundles were incorporated into the composite of HA and PLGA to obtain a biodegradable and traceable bone implant for MRI and X-ray tracing. After the toxicity and bioactivity test of nanocomposite in vitro, $GdPO_4 \cdot H_2O$ nanobundles were successfully proposed as a tracer and contrast agent in HA/PLGA materials for X-ray CT and MRI application by animal test (**Scheme 1**). The as-prepared $GdPO_4 \cdot H_2O$ nanobundles were of ≈1 μm in length and ≈30 nm in width with pure hexagonal structure and no impurity phase, exhibiting higher magnetism compared to the calcinated $GdPO_4$. HA/PLGA composite implants containing $GdPO_4 \cdot H_2O$ could be easily and efficiently monitored by MRI when the concentration of $GdPO_4 \cdot H_2O$ in $GdPO_4 \cdot H_2O$/HA/PLGA implants (w/w) was more than 0.33% due to the Gd paramagnetism. Its CT imaging was fainter at the same concentration of $GdPO_4 \cdot H_2O$ in $GdPO_4 \cdot H_2O$/HA/PLGA implants (w/w) but clearly enhanced after new bone formation. The implants and the newly formed bones could be easily traced and observed through the combination of MRI and X-ray imaging. No significant cytotoxicity

Dr. J. Huang, Prof. H. Zou
College of Chemistry
Jilin University
Changchun 130012, P. R. China
E-mail: zouhf@jlu.edu.cn
Dr. J. Huang, Dr. Y. Wang, Dr. Z. Wang, Dr. T. Gao, Dr. M. Guo, Prof. P. Zhang
Key Laboratory of Polymer Ecomaterials
Changchun Institute of Applied Chemistry
Chinese Academy of Sciences
Changchun 130022, P. R. China
E-mail: zhangpb@ciac.ac.cn
Z. Lv
China-Japan Union Hospital
Jilin University
Changchun 130021, P. R. China
Dr. T. Gao
School of Public Health
Jilin University
Changchun 130021, P. R. China
Dr. N. Zhang
Department of Foot and Ankle Surgery
The Second Hospital of Shandong University
Jinan 250000, P. R. China

DOI: 10.1002/adhm.201600249

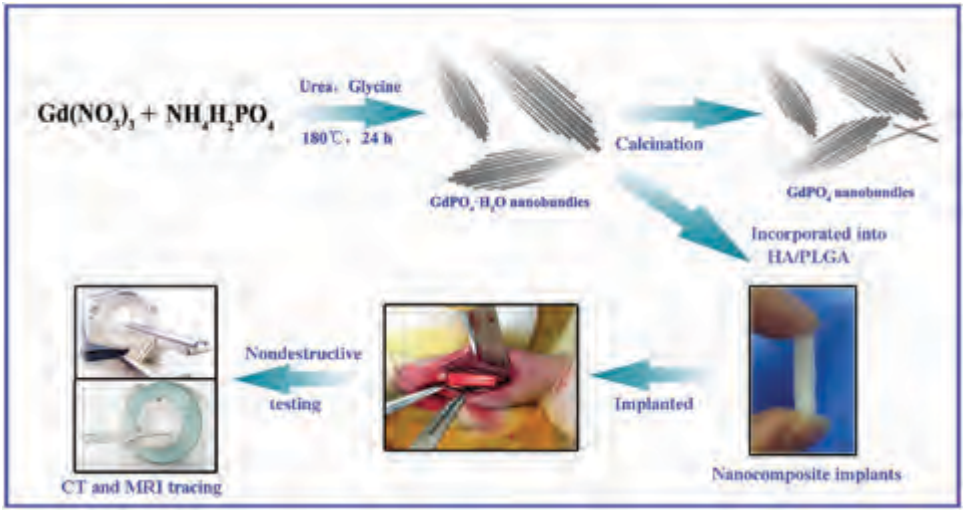

Scheme 1. Schematic illustration of $GdPO_4{\cdot}H_2O$ and $GdPO_4$ nanobundles synthesis and their application in biodegradable bone implants for MR and CT tracing.

was observed and the expression of osteocalcin was clearly promoted at the proper $GdPO_4{\cdot}H_2O$ concentration, indicating a potential application in the traceable polymeric orthopedic implants.

Figure 1A,B shows the XRD patterns of the as-prepared $GdPO_4{\cdot}H_2O$ (A) and $GdPO_4$ (B) products and their corresponding standard data. All the diffraction peaks in Figure 1A indicated that the precursor [space group: P3121 (152)] cell parameters a = 0.6891 nm and c = 0.6356 nm could be clearly associated to the hexagonal $GdPO_4{\cdot}H_2O$ phase (JCPDS No. 39–0232). After calcination at 800 °C, the XRD of calcinate in Figure 1B [space group: P21/n (14)] with cell parameters of a = 6.61847 nm, b = 0.6819 nm, and c = 0.6318 nm could be associated with the $GdPO_4$ monoclinic phase (JCPDS No. 32–0386), meaning that the precursor was completely transformed into the monoclinic phase due to the removal of crystal H_2O from the hexagonal phase.[12] The characteristic diffraction peaks of both samples were sharp and narrow, suggesting that the obtained $GdPO_4{\cdot}H_2O$ and $GdPO_4$ were pure with a high crystallinity.[13]

The FT-IR spectra of both the as-prepared $GdPO_4{\cdot}H_2O$ and $GdPO_4$ nanomaterials are shown in Figure 1C. The band at 1077 cm^{-1} in the $GdPO_4{\cdot}H_2O$ spectrum represented a characteristic asymmetry stretch vibration of the P—O. Bands located at 623 and 544 cm^{-1} were due to the O—P—O bend vibration in the PO_4^{3-} groups, indicating that the samples were in the hexagonal morphology of rare earth orthophosphate with eight ligands. The absorption bands at 1404 cm^{-1} belonged to the CH_2 scissor bending vibration because of the presence of residual ethanol.[14] Bands around 1617 and 3500 cm^{-1} were ascribed to hydration water (O—H bond) in the as-prepared powders of both the two compounds.[15] The spectrum of $GdPO_4$ showed weaker absorptions at 1617 and 3500 cm^{-1} due to the removal of hydration water after calcination, compared with $GdPO_4{\cdot}H_2O$. The other bands present in the FT-IR spectrum of $GdPO_4$ belonged to the phosphate groups. The split bands at 1077, 1007, and 967 cm^{-1} in the $GdPO_4$ spectrum were characteristic of the monoclinic $GdPO_4$ phase (phosphate P—O stretching).[15,16] The vibration spectra gave a conclusive evidence of the $GdPO_4$ monoclinic-phase formation.[16]

A typical TG-DTA analysis of the $GdPO_4{\cdot}H_2O$ (black line) and $GdPO_4$ (red line) nanomaterials was observed under nitrogen gas flow, as shown in Figure 1D. $GdPO_4{\cdot}H_2O$ TG curve exhibited two weight losses with an overall loss of 6.7%. The first weight loss at 25–140 °C was due to the removal of the absorbed water (≈0.8%) and the second loss at 140–800 °C was mainly due to the decomposition of the crystal water (≈5.9%). The weight loss phenomenon we observed is similar to the literature.[7,17] In contrast, $GdPO_4$ TG curve showed two weight losses with an overall loss of 1.1%: a small continuous weight loss (≈0.4%) at 25–140 °C which was corresponding to the water release from the particles' surface and the second weight loss (≈0.7%) began at approximately 140 °C and might correspond to the release of the water molecules entrapped in the channels of the monoclinic lattice.[18] According to the DTA curve in Figure 1D, the $GdPO_4{\cdot}H_2O$ had a relatively weak endothermic peak at 140–180 °C probably related with the massive decomposition of crystal water and more heat absorption.

Figure 1E (a and e) shows $GdPO_4{\cdot}H_2O$ and $GdPO_4$ SEM (scanning electron microscope) images, respectively. It is shown that the product prepared under different conditions were bundle-like nanoparticles. Most of the $GdPO_4{\cdot}H_2O$ and $GdPO_4$ nanobundles were composed of many regular and stagger nanorods with an average particle size of ≈1 μm in length and ≈30 nm in width. The marked difference, however, some $GdPO_4$ nanobundles were fractured due to the removal of crystal water and the change of crystal structure, as shown in Figure 1E (e).

Figure 1E also shows TEM (transission electron microscope), HRTEM (high resolution transmission electron microscope), SAED (selected area electron diffraction) images of $GdPO_4{\cdot}H_2O$ (b–d) and $GdPO_4$ (f–h) nanobundles. TEM images further confirmed that both of them consisted of many nanowires, and $GdPO_4$ exhibited more inhomogeneous size and morphology compared to $GdPO_4{\cdot}H_2O$. $GdPO_4{\cdot}H_2O$ and $GdPO_4$ fringe spacing was 0.345 and 0.338 nm, respectively.

Adv. Healthcare Mater. **2016**,
DOI: 10.1002/adhm.201600249

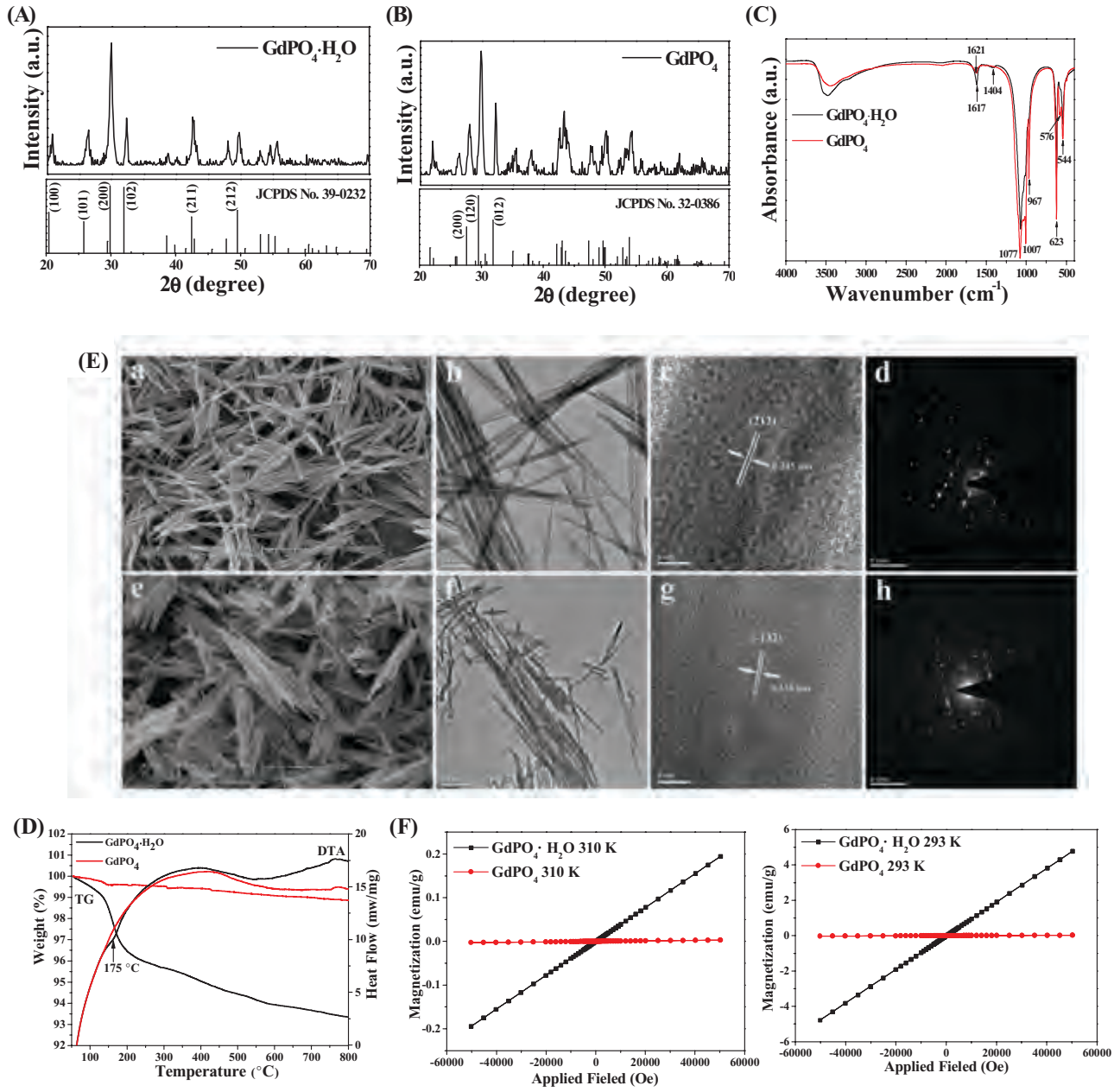

Figure 1. A) XRD pattern of $GdPO_4{\cdot}H_2O$ nanobundles. B) XRD pattern of $GdPO_4$ nanobundles. C) FT-IR spectra of $GdPO_4{\cdot}H_2O$ and $GdPO_4$ nanobundles. D) TG–DTA curves of $GdPO_4{\cdot}H_2O$ and $GdPO_4$ nanobundles. E) Morphologic analysis of $GdPO_4{\cdot}H_2O$ (a–d) and $GdPO_4$ (e–h) nanobundles with SEM (a and e), TEM (b and f), HRTEM (c and g), and SAED (d and h) images. F) Magnetization plots of $GdPO_4{\cdot}H_2O$ and $GdPO_4$ nanobundles at the temperature of 293 and 310 K, respectively.

They were in good agreement with those of the (212) and (–132) planes of the JCPDS No. 39–0232 ($GdPO_4{\cdot}H_2O$, hexagonal phase) and JCPDS No. 32–0386 ($GdPO_4$, monoclinic phase). SAED analysis indicated that the products of both $GdPO_4{\cdot}H_2O$ and $GdPO_4$ were monocrystals.

Due to the half-filled f-orbital with seven electrons, Gd^{3+} ions possess a high magnetic moment, leading to clear effects on both longitudinal and transverse proton relaxation even at low applied magnetic fields.[19] Thus, Gd-containing materials have signal enhancement ability and can be potentially applied in clinical imaging as MRI contrast agents. Figure 1F shows the magnetic plots of $GdPO_4{\cdot}H_2O$ and $GdPO_4$ nanobundles at the temperature of 293 and 310 K. $GdPO_4{\cdot}H_2O$ nanobundles exhibited a stronger paramagnetic behavior, suggesting that $GdPO_4{\cdot}H_2O$ dehydration might change the structure and gadolinium ions in a low-spin state.[20]

Figure 2A shows MRI and CT imagings of HA/PLGA implants containing increasing $GdPO_4{\cdot}H_2O$ or $GdPO_4$ concentrations (range 0%–2.60%, w/w) tested in vitro in PBS solution, in order to evaluate and select a more proper density of contrast agents.

MRI imaging showed that the signals of both the two implants were increased in a concentration-dependent manner

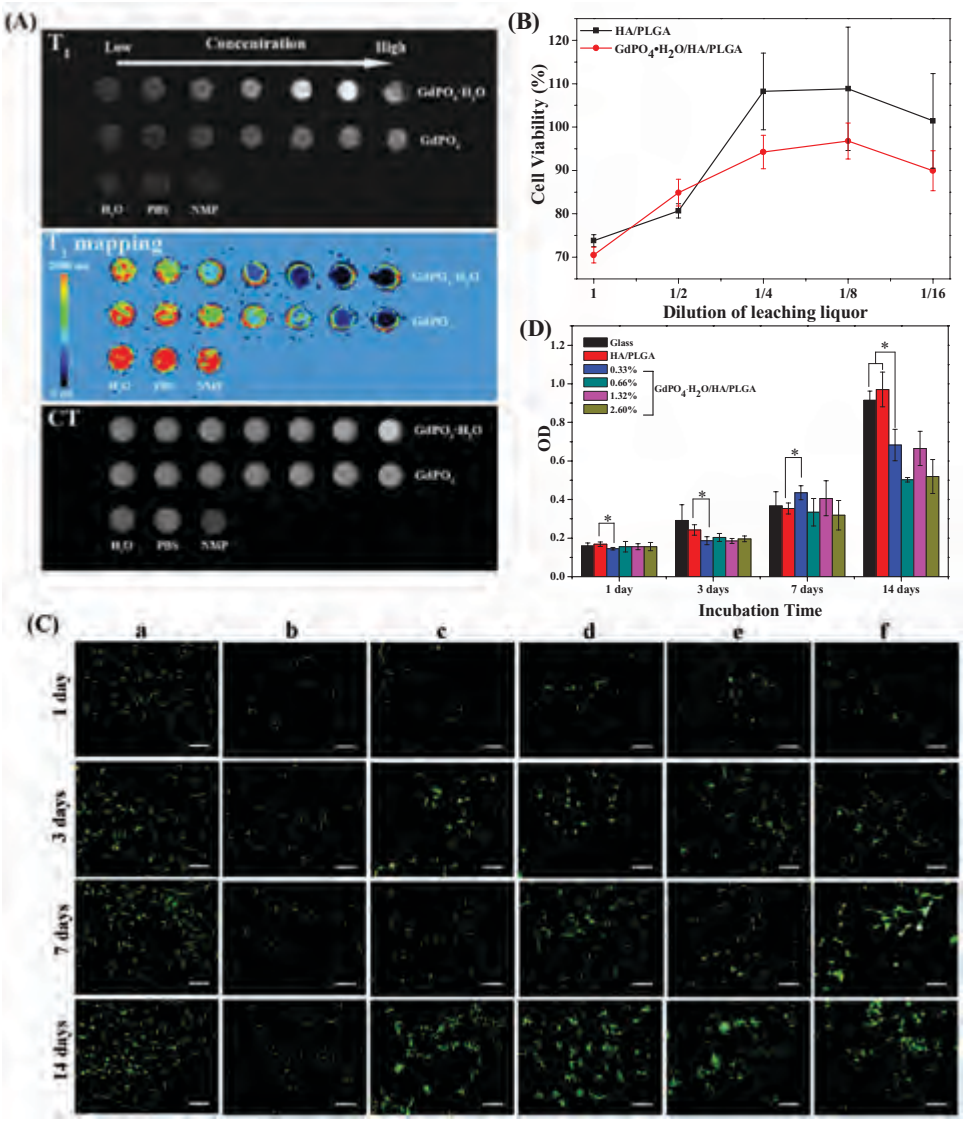

Figure 2. A) T_1-weighted images, parametric mapping and X-ray CT images of HA/PLGA implants incorporated with $GdPO_4{\cdot}H_2O$ and $GdPO_4$ nanobundles at the concentrations of 0, 0.08%, 0.17%, 0.33%, 0.66%, 1.32%, and 2.60% (w/w) from left to right, respectively. B) Cytotoxicity of material's leaching liquor on MC3T3-E1 determined by CCK-8 assay. C) MC3T3-E1 cell adhesion on different substrates for 1, 3, 7, and 14 d: (a) Glass; (b) HA/PLGA; (c–f) $GdPO_4{\cdot}H_2O$/HA/PLGA with different $GdPO_4{\cdot}H_2O$ concentrations such as 0.33%, 0.66%, 1.32%, and 2.60% (w/w). Bar = 100 μm. D) MC3T3-E1 osteoblast proliferation analysis on different substrates by CCK-8 assay, $^*p < 0.05$.

on the T_1-weighted images. As expected, the implants containing $GdPO_4{\cdot}H_2O$ possess a higher signal enhancement due to their stronger magnetism according to the results in Figure 1F, suggesting that the concentration of 0.33%–2.60% $GdPO_4{\cdot}H_2O$ can be selected for the in vivo MR imaging of HA/PLGA implants.

In addition, $GdPO_4{\cdot}H_2O$ and $GdPO_4$ showed a specific enhancement also on CT imaging in HA/PLGA implants when their concentrations were 0.66%–2.60%. This result could be due to a stronger X-ray attenuation and higher gadolinium atomic number.[21]

To verify if the $GdPO_4{\cdot}H_2O$ nanobundles could be used in biomedicine, $GdPO_4{\cdot}H_2O$/HA/PLGA cytotoxicity test was essential. As shown in Figure 2B, the cytotoxicity of the leaching liquors of 6 cm^2 mL^{-1} HA/PLGA and $GdPO_4{\cdot}H_2O$/HA/PLGA containing the highest concentration of $GdPO_4{\cdot}H_2O$ (2.60%, w/w) was tested in the MC3T3-E1 cells. The viability of the cells treated with HA/PLGA and $GdPO_4{\cdot}H_2O$/HA/PLGA original leaching liquors were 73.8 ± 1.4% and 70.5 ± 1.8%, respectively. There was only a little decrease in cell viability for $GdPO_4{\cdot}H_2O$/HA/PLGA compared to HA/PLGA. The cell viabilities treated with the two materials remarkably increased when the leaching liquors were two- or fourfold diluted. With more than fourfold dilution, the viability of the cells treated with HA/PLGA was higher than the blank control (>100%) and ≈15% higher than that of $GdPO_4{\cdot}H_2O$/HA/PLGA. The results indicated that some ingredients in HA ceramics were improving cell viability.[7] Therefore, $GdPO_4{\cdot}H_2O$/HA/PLGA toxic effects caused by the incorporation of $GdPO_4{\cdot}H_2O$ were scarce and negligible. Meanwhile, the literature has reported similar in vitro

Adv. Healthcare Mater. 2016,
DOI: 10.1002/adhm.201600249

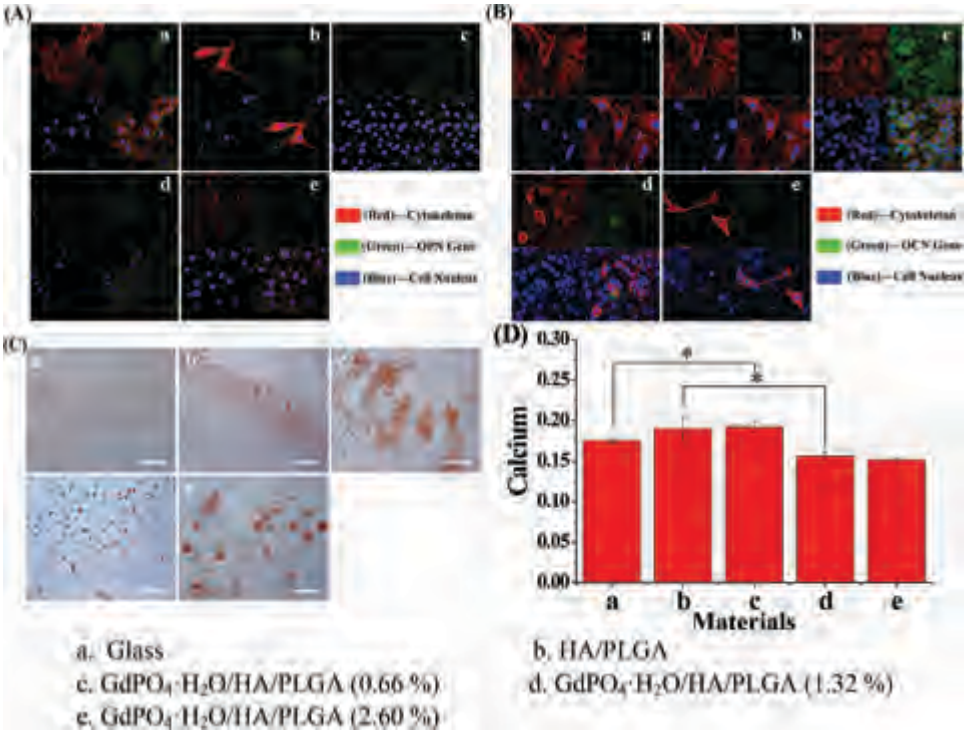

Figure 3. A) OPN immunofluorescence staining in MC3T3-E1 cells cultured for 9 d on different substrates. B) OCN immunofluorescence staining in MC3T3-E1 cells cultured for 9 d on different substrates. C) Alizarin Red staining (a–e) and D) the corresponding quantitative evaluation of calcium content mineral deposition in MC3T3-E1 cells cultured for three weeks. Bar = 200 μm, $*p < 0.05$.

cyto-biocompatibility of $GdPO_4$ nanorods and $GdPO_4$ nanocubes when cells were cultured with these nanomaterials.[9]

In addition to the absence of toxicity, an ideal scaffold material should possess a biological activity such as allow cell attachment, spreading and proliferation.[22] Figure 2C shows the images of MC3T3-E1 cells grown on different substrates, such as glass, HA/PLGA and $GdPO_4 \cdot H_2O$/HA/PLGA at increasing concentrations (0.33%, 0.66%, 1.32%, and 2.60%, w/w) for 1, 3, 7, and 14 d. The cells on the glass substrate initially attached and spread better than those on HA/PLGA and $GdPO_4 \cdot H_2O$/HA/PLGA composites after 1 d of culture. After 3 d of culture, the cells on both HA/PLGA and $GdPO_4 \cdot H_2O$/HA/PLGA substrates begin to attach and actively spread. When cultured for 7–14 d, the morphology of cells on the $GdPO_4 \cdot H_2O$/HA/PLGA substrates were changed when compared to the cells on HA/PLGA. These results suggested that $GdPO_4 \cdot H_2O$ incorporation was beneficial for the spreading of osteoblasts.

MC3T3-E1 cell proliferation on the different materials using CCK-8 assay is shown in Figure 2D. When cultured for 1 d, the osteoblasts number was similar among all the materials. After 3 d of culture, the cell number on glass and HA/PLGA were higher than those on $GdPO_4 \cdot H_2O$/HA/PLGA composites. After 7 d of culture, the cell number on $GdPO_4 \cdot H_2O$/HA/PLGA (0.33%, w/w) was significantly higher than that on HA/PLGA group, indicating that a small $GdPO_4 \cdot H_2O$ amount might improve cell proliferation. After 14 d of culture, the cell number on glass and HA/PLGA were clearly higher than those on $GdPO_4 \cdot H_2O$/HA/PLGA groups due to the HA's ingredients contribution to proliferation[5] or some $GdPO_4 \cdot H_2O$ ingredients inducing the osteoblasts morphological change shown in Figure 2C that might be associated to osteoblast differentiation.

To study the effect of $GdPO_4 \cdot H_2O$ nanomaterials on early phase of osteoblast differentiation, the immunofluorescence staining of the osteogenic markers was performed and analyzed by CLSM (**Figure 3**A,B). MC3T3-E1 cells were cultured on different substrates, such as glass, HA/PLGA and $GdPO_4 \cdot H_2O$/HA/PLGA (0.66%, 1.32%, and 2.60%, w/w) for 9 d. Among the osteogenic markers, OCN is the most abundant protein in bone and is exclusively produced by osteoblasts.[23] OPN is an important noncollagen protein that enables bone cells to adhere to the mineralized matrix and play a key role in the mineralization process.[24] After 9 d of culture, MC3T3-E1 cells cultured on different substrates did not show any OPN immunofluorescence staining difference indicating no different OPN expression (Figure 3A). However, OCN expression in MC3T3-E1 cells was increased in the $GdPO_4 \cdot H_2O$/HA/PLGA groups compared to the glass (Figure 3B). OCN expression was most pronounced when $GdPO_4 \cdot H_2O$ concentration in $GdPO_4 \cdot H_2O$/HA/PLGA was 0.66% (w/w). These results indicated that the $GdPO_4 \cdot H_2O$ nanobundles in a proper concentration could enhance the expression of osteocalcin in MC3T3-E1 cells, which might induce a subsequent promotion of osteoblast mineralization. According to the relative researches, we knew that phosphate has a high degree of specificity in the signaling mechanism and can selectively activate the extracellular signal regulated kinase (ERK1/2) signaling pathway. After that, the phosphate may increase transcription of osteogenic protein and induce osteogenic protein expression.[25]

Figure 3C shows the optical microscopic images of MC3T3-E1 cells Alizarin Red staining on glass, HA/PLGA and $GdPO_4 \cdot H_2O$/HA/PLGA at the concentration of 0.66%, 1.32%, and 2.60% (w/w) at three weeks. After treatment with Alizarin Red staining, calcium-rich deposits were evaluated in MC3T3-E1 cells by Alizarin Red binding with Ca^{2+} in mineralized ECM.[26] The red calcium nodules in MC3T3-E1 cells on $GdPO_4 \cdot H_2O$/HA/PLGA substrates (c–e) were increased compared with the cells growing on glass and HA/PLGA (a and b).

The assessment of quantitative cell mineralization was performed by extracting Alizarin Red with 10% cetylpyridinium chloride (CPC) to evaluate calcium-rich mineral deposits (Figure 3D). Calcium quantification was recorded as total calcium content and normalized to cell number. The calcium content in MC3T3-E1 cells on 0.66% $GdPO_4 \cdot H_2O$/HA/PLGA substrate was significantly higher than that of cells growing on the other materials. The quantitative assessment of mineral deposition showed the same trend of the osteogenic protein expression of OCN (Figure 3B), indicating that the proper concentration of $GdPO_4 \cdot H_2O$ nanobundles promoted the mineralization process in MC3T3-E1 cells. The reason may be that $GdPO_4 \cdot H_2O$ could provide more inorganic phosphates as cell-communicating ingredients acting as signaling molecules in osteoblast differentiation to regulate protein expression, thus promoting autocalcification.[10,25]

T_1 MRI images and their parametric mapping of rabbit radius defects after implanted with PLGA, HA/PLGA, and $GdPO_4 \cdot H_2O$/HA/PLGA for 0–8 weeks are shown in **Figure 4**A. As shown in Figure 4A, PLGA and HA/PLGA implants were not or hardly detected in the rabbit radius at 0 week. However, the composites containing $GdPO_4 \cdot H_2O$ could be more easily detected when its concentration was more than 0.66%, with an increasing signal intensities by increasing $GdPO_4 \cdot H_2O$ concentration thanks to more paramagnetic Gd^{3+} interactions with water protons.[27]

As shown in Figure 4B, the CT signals linearly increased with increasing $GdPO_4 \cdot H_2O$ concentration in the PLGA due to a higher attenuation of Gd in X-ray, but they were fainter than those in MRI especially at the initial stages after implantation. The implants containing $GdPO_4 \cdot H_2O$ nanobundles could be easier recognized than PLGA and HA/PLGA, suggesting that $GdPO_4 \cdot H_2O$/HA/PLGA could be also recognized using X-ray CT imaging.

Furthermore, the CT signals of composite implants were gradually enhanced at two and eight weeks after implantation, especially in the $GdPO_4 \cdot H_2O$/HA/PLGA at different concentration of Gd. These results might be related to the new bone formation according to the CT images 3D reconstruction (Figure 4B). Thus, although $GdPO_4 \cdot H_2O$ CT imaging is less visible than its MRI imaging at the initial stage after implantation, the combined MRI and CT imaging used to trace $GdPO_4 \cdot H_2O$ implants might really represent the changes of implants and a novelty in the guided bone ingrowth monitoring at different stages.

Figure 4C shows a histological study of the repaired areas performed with H&E and Masson trichrome staining at eight weeks after implantation. Using Masson trichrome staining, collagen fibers and osteoids could be distinguished in green and red.[28] In the PLGA group, the cells encompassed the materials and the new bone formation was inhibited due to hydrophobicity of PLGA. However, a visible new bone spur was formed around the side of HA/PLGA group (3D reconstruction CT images in Figure 4B), which could further verify the improvement of bone growth ability for HA. For $GdPO_4 \cdot H_2O$/HA/PLGA implants, although the slight inflammatory reaction in the defect area was caused by $GdPO_4 \cdot H_2O$/HA/PLGA (1.32%, w/w) due to the increased incorporation of gadolinium compound, cells were more willing to creep into the internal of materials, the materials were more easily decomposed into small pieces and then there were many collagen fibers around/in materials. Combining with the CT images, the $GdPO_4 \cdot H_2O$/HA/PLGA implants could be easily detected due to the increasing density with time, which may further prove the $GdPO_4 \cdot H_2O$/HA/PLGA materials in bone defect showed faster bone regeneration than other groups. Therefore, these results demonstrated that the appropriate dosage of $GdPO_4 \cdot H_2O$ in HA/PLGA could promote ossein secretion and improve bone regeneration.

After eight weeks implantation for rabbit, the inflammation or tissue damage of $GdPO_4 \cdot H_2O$/HA/PLGA to viscera (heart, liver, spleen, and kidney) was assessed by H&E staining in Figure S1 of the Supporting Information. Compared to the untreated group, some faint inflammation effects on kidney were observed due to the high concentration of $GdPO_4 \cdot H_2O$ in implant, while no inflammation was observed in the other tissues.

Just like many other kinds of drugs, $GdPO_4 \cdot H_2O$ also possesses a dose-dependent relationships between bioactivity and toxicity. Some gadolinium compounds show their adverse bioeffects at high dose.[29,30] Especially by intraperitoneal or intravenous injection, the micro/nanomaterials might be easily absorbed and metabolized by the liver and kidney through blood, and then more likely produce toxic effects in vivo. Slight adverse bioeffect of $GdPO_4 \cdot H_2O$ at high dose in HA/PLGA were also observed in present study. But in the case of lower dosage, the effect on attachment, spreading and proliferation of osteoblast was still guaranteed at $GdPO_4 \cdot H_2O$ low concentrations. All inorganic nanoparticles are hard to be rapidly released due to the encompassment of biodegradable polymer composites and then they will result in less toxicity to body. In practice, $GdPO_4 \cdot H_2O$/HA/PLGA implants could better exert their role and be used in vivo more efficiently when the proper amount of $GdPO_4 \cdot H_2O$ in HA/PLGA was used.

$GdPO_4 \cdot H_2O$ seems to benefit osteoblast's differentiation and biomineralization. Through the cell experiments in vitro and animal test in vivo, the protein expression results, cell mineralization experiment, and histological analysis proved that the proper amount of $GdPO_4 \cdot H_2O$ in HA/PLGA could induce OCN expression in MC3T3-E1 cells, facilitate the mineralization process and promote bone formation. The bioactivities of several rare earth elements for bone regeneration have been reported.[29,31] Lanthanide oxides in bioactive glass enhance the production of collagen in HMSCs (Human Mesenchymal Stem Cells).[29] On the other hand, lanthanide ions can promote bone resorption at lower concentrations, but turn to inhibit bone resorption at higher concentrations.[31] It might be related to their direct action on bone surface and incorporation in the hydroxyapatite,[31] as well as their

Adv. Healthcare Mater. **2016**,
DOI: 10.1002/adhm.201600249

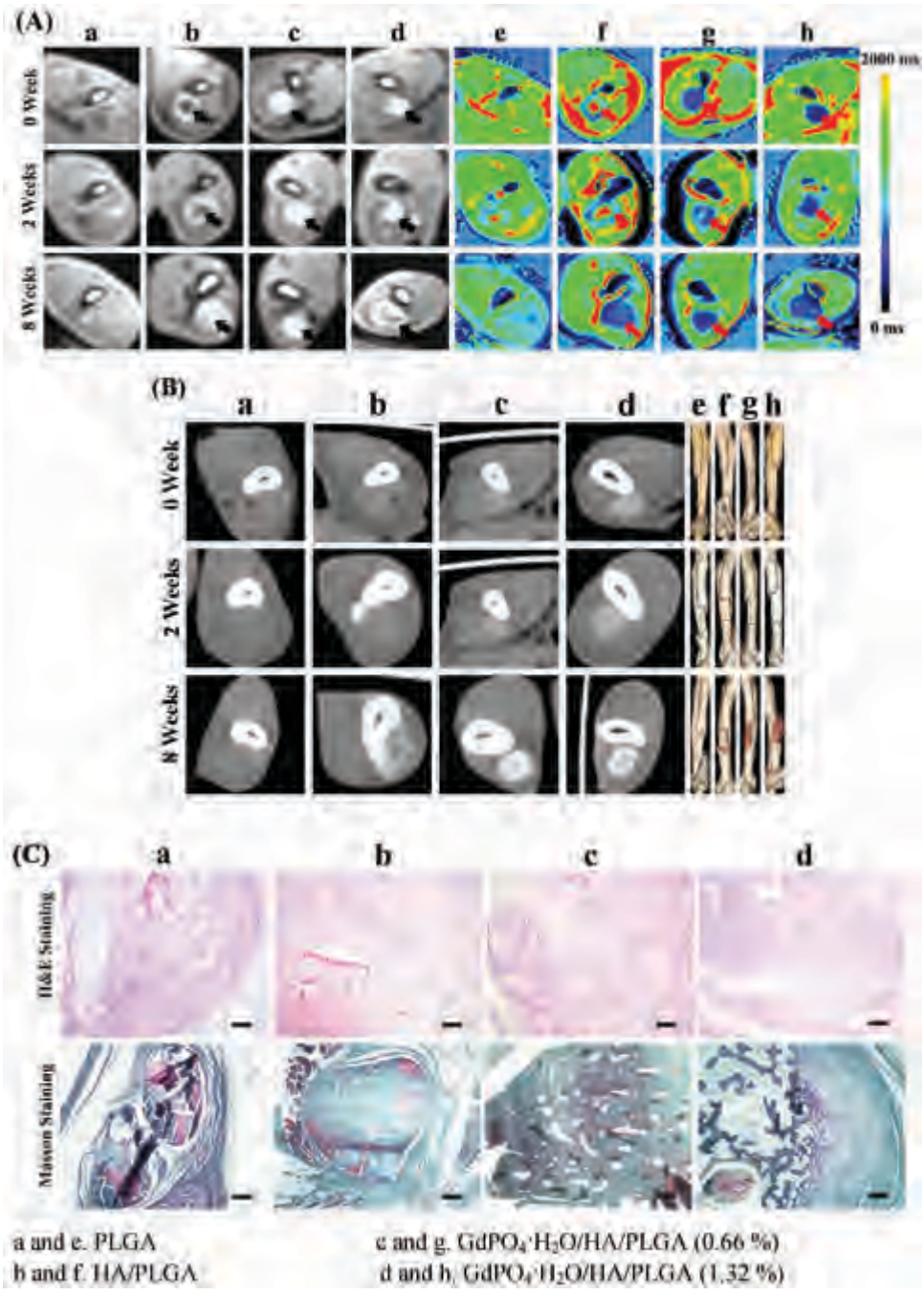

Figure 4. A) T_1 MRI images (a–d) and their parametric mapping (e–h) of rabbit radius defects implanted with different materials for 0, 2, and 8 weeks. B) X-ray CT images (a–d) and 3D reconstruction CT images (e–h) of rabbit radius defects implanted with different materials for 0, 2, and 8 weeks. C) H&E and Masson trichrome staining of cross sections of rabbit radius defects implanted for 8 weeks. Bar = 200 μm.

bidirectional effects on intracellular calcium ion concentration by activating a membrane-bound Ca^{2+}-sensing receptor or blocking calcium channel.[32] Besides, the introduction of PO_4^{3-} in this study is another key factor for enhancing bone growth because of its role as a specific signal for osteogenic protein expression.[10]

In summary, our results suggest that the appropriate amount of $GdPO_4 \cdot H_2O$ in HA/PLGA implants could be used as a contrast agent for MRI tracing and CT imaging. The combination of MRI and CT imaging could efficiently monitor the implants modifications at different stages because the CT imaging of $GdPO_4 \cdot H_2O$ was less visible than its MRI imaging at the initial stage after implantation and was clearly enhanced by new bone formation at the subsequent stages. Thus, this imaging combination provided a feasible approach to observe polymeric implants in a noninvasive way. We have successfully synthesized the well dispersed and homogeneous $GdPO_4 \cdot H_2O$ nanobundles via solvothermal method

using MRI or X-ray contrast agent applied in biodegradable HA/PLGA bone implants. The as-prepared $GdPO_4 \cdot H_2O$ was in a pure hexagonal phase and bundle products, and had a higher magnetism than the calcined $GdPO_4$. In addition, $GdPO_4 \cdot H_2O$ incorporated in the HA/PLGA had better effects as contrast agents using MR and X-ray imaging compared to $GdPO_4$. The in vitro biological assessments indicated that the proper $GdPO_4 \cdot H_2O$ nanobundles could promote the expression of OCN and mineralization of the osteoblasts although their proliferation were inhibited after in vitro culture for two weeks. When implanted in vivo, the distinct differences in MRI and CT imaging densities on $GdPO_4 \cdot H_2O$ at the initial stage of implantation and the following enhanced X-ray due to bone regeneration provided an effective approach for recognizing the implants or the newly formed bone tissues. Furthermore, MRI, CT, and histological analysis results indicated that the proper dose of $GdPO_4 \cdot H_2O$ in HA/PLGA promoted bone formation and enhanced osseointegration between implant and bone. Our work thus suggests that $GdPO_4 \cdot H_2O$ nanobundles may be widely applied in polymers or their composites for traceable bone implants, bone fixing materials and tissue engineering scaffolds using MRI and X-ray imaging combination to provide a feasible approach to observe polymeric implants in a noninvasive way.

Supporting Information

Supporting Information is available from the Wiley Online Library or from the author.

Acknowledgements

This work was supported by the National Natural Science Foundation of China (Nos. 51473164, 51403197, and 51273195), the Ministry of Science and Technology of China (International Cooperation and Communication Program 2014DFG52510), the Program of Scientific Development of Jilin Province (20130201005GX), and the Joint funded program of Chinese Academy of Sciences and Japan Society for the Promotion of Science (GJHZ1519). All animal procedures were in agreement with the guidelines of the Regional Ethics Committee for Animal Experiments established by Jilin University Institutional Animal Care and Use.

Received: March 8, 2016
Revised: June 6, 2016
Published online:

[1] a) J. Li, Y. Hu, J. Yang, P. Wei, W. Sun, M. Shen, G. Zhang, X. Shi, *Biomaterials* **2015**, *38*, 10; b) Q. Chen, H. Wang, H. Liu, S. Wen, C. Peng, M. Shen, G. Zhang, X. Shi, *Anal. Chem.* **2015**, *87*, 3949; c) J. Yu, C. Yang, J. Li, Y. Ding, L. Zhang, M. Z. Yousaf, J. Lin, R. Pang, L. Wei, L. Xu, F. Sheng, C. Li, G. Li, L. Zhao, Y. Hou, *Adv. Mater.* **2014**, *26*, 4114; d) J. Li, Y. He, W. Sun, Y. Luo, H. Cai, Y. Pan, M. Shen, J. Xia, X. Shi, *Biomaterials* **2014**, *35*, 3666; e) H. Yang, Y. Zhuang, Y. Sun, A. Dai, X. Shi, D. Wu, F. Li, H. Hu, S. Yang, *Biomaterials* **2011**, *32*, 4584.

[2] Z. Cao, Q. Yu, H. Xue, G. Cheng, S. Jiang, *Angew. Chem.* **2010**, *49*, 3771.

[3] a) W. Chen, T. Long, Y.-J. Guo, Z.-A. Zhu, Y.-P. Guo, *RSC Adv.* **2014**, *4*, 185; b) K. Du, X. Shi, Z. Gan, *Langmuir* **2013**, *29*, 15293; c) J. D. Chen, Y. J. Wang, K. Wei, S. H. Zhang, X. T. Shi, *Biomaterials* **2007**, *28*, 2275.

[4] a) C. V. M. Rodrigues, P. Serricella, A. B. R. Linhares, R. M. Guerdes, R. Borojevic, M. A. Rossi, M. E. L. Duarte, M. Farina, *Biomaterials* **2003**, *24*, 4987; b) V. Brun, C. Guillaume, S. M. Alami, J. Josse, J. Jing, F. Draux, S. Bouthors, D. Laurent-Maquin, S. C. Gangloff, H. Kerdjoudj, F. Velard, *Bio-Med. Mater. Eng.* **2014**, *24*, S63; c) E. Nejati, V. Firouzdor, M. B. Eslaminejad, F. Bagheri, *Mater. Sci. Eng., C* **2009**, *29*, 942; d) S. S. Kim, M. S. Park, O. Jeon, C. Y. Choi, B. S. Kim, *Biomaterials* **2006**, *27*, 1399.

[5] P. Zhang, Z. Hong, T. Yu, X. Chen, X. Jing, *Biomaterials* **2009**, *30*, 58.

[6] a) D. Li, C. Ye, Y. Zhu, Y. Y. Qi, Z. R. Gou, C. Y. Gao, *Polym. Adv. Technol.* **2012**, *23*, 1446; b) L. H. Lao, Y. J. Wang, Y. Zhu, Y. Y. Zhang, C. Y. Gao, *J. Mater. Sci.* **2011**, *22*, 1873.

[7] P. Zhang, H. Wu, H. Wu, Z. Lu, C. Deng, Z. Hong, X. Jing, X. Chen, *Biomacromolecules* **2011**, *12*, 2667.

[8] a) S. Comby, E. M. Surender, O. Kotova, L. K. Truman, J. K. Molloy, T. Gunnlaugsson, *Inorg. Chem.* **2014**, *53*, 1867; b) F. Liu, X. He, L. Liu, H. You, H. Zhang, Z. Wang, *Biomaterials* **2013**, *34*, 5218; c) C.-C. Huang, C.-H. Su, W.-M. Li, T.-Y. Liu, J.-H. Chen, C.-S. Yeh, *Adv. Funct. Mater.* **2009**, *19*, 249.

[9] a) S. Rodriguez-Liviano, A. I. Becerro, D. Alcantara, V. Grazu, J. M. de la Fuente, M. Ocana, *Inorg. Chem.* **2013**, *52*, 647; b) W. L. Ren, G. Tian, L. J. Zhou, W. Y. Yin, L. Yan, S. Jin, Y. Zu, S. J. Li, Z. J. Gu, Y. L. Zhao, *Nanoscale* **2012**, *4*, 3754.

[10] a) G. R. Beck Jr., B. Zerler, E. Moran, *Proc. Natl. Acad. Sci. USA* **2000**, *97*, 8352; b) Y. R. V. Shih, Y. Hwang, A. Phadke, H. Kang, N. S. Hwang, E. J. Caro, S. Nguyen, M. Siu, E. A. Theodorakis, N. C. Gianneschi, K. S. Vecchio, S. Chien, O. K. Lee, S. Varghese, *Proc. Natl. Acad. Sci. USA* **2014**, *111*, 990.

[11] J. Caverzasio, T. Selz, J. P. Bonjour, *Calcif. Tissue Int.* **1988**, *43*, 83.

[12] H. Lai, X. Yang, H. Yang, *J. Mater. Sci.: Mater. Electron.* **2011**, *23*, 285.

[13] A. Janner, T. Janssen, P. M. Dewolff, *Acta Crystallogr., A* **1983**, *39*, 667.

[14] Y.-Y. Fan, Z.-C. Hu, J. Yang, C. Zhang, L. Zhu, *Appl. Surf. Sci.* **2013**, *266*, 22.

[15] H. J. Song, L. Q. Zhou, L. Li, F. Hong, X. R. Luo, *Mater. Res. Bull.* **2013**, *48*, 5013.

[16] Y. Yang, *Mater. Sci. Eng.: B* **2013**, *178*, 807.

[17] S. Z. Lu, J. H. Zhang, J. S. Zhang, H. F. Zhao, Y. S. Luo, X. G. Ren, *Nanotechnology* **2010**, *21*, 2431.

[18] A. I. Becerro, S. Rodriguez-Liviano, A. J. Fernandez-Carrion, M. Ocana, *Cryst. Growth Des.* **2013**, *13*, 526.

[19] F. Chen, P. Huang, Y. J. Zhu, J. Wu, D. X. Cui, *Biomaterials* **2012**, *33*, 6447.

[20] W. Ouellette, A. V. Prosvirin, K. Whitenack, K. R. Dunbar, J. Zubieta, *Angew. Chem.* **2009**, *48*, 2140.

[21] a) Z. Liu, F. Pu, S. Huang, Q. Yuan, J. Ren, X. Qu, *Biomaterials* **2013**, *34*, 1712; b) Q. Chen, K. Li, S. Wen, H. Liu, C. Peng, H. Cai, M. Shen, G. Zhang, X. Shi, *Biomaterials* **2013**, *34*, 5200.

[22] a) K. Anselme, *Biomaterials* **2000**, *21*, 667; b) S. Verrier, J. J. Blaker, V. Maquet, L. L. Hench, A. R. Boccaccini, *Biomaterials* **2004**, *25*, 3013.

[23] M. L. Zoch, T. L. Clemens, R. C. Riddle, *Bone* **2015**, *82*, 42.

[24] M. Morinobu, M. Ishijima, S. R. Rittling, K. Tsuji, H. Yamamoto, A. Nifuji, D. T. Denhardt, M. Noda, *J. Bone Miner. Res.* **2003**, *18*, 1706.

[25] a) G. R. Beck Jr., *J. Cell. Biochem.* **2003**, *90*, 234; b) F. R. Maia, S. J. Bidarra, P. L. Granja, C. C. Barrias, *Acta Biomater.* **2013**, *9*, 8773.
[26] G. J. Lai, K. T. Shalumon, S. H. Chen, J. P. Chen, *Carbohydr. Polym.* **2014**, *111*, 288.
[27] Y. Sun, X. Zhu, J. Peng, F. Li, *ACS Nano* **2013**, *7*, 11290.
[28] a) S. N. Asonova, N. S. Migalkin, *Arkh. Patol.* **1996**, *58*, 66; b) W. J. Cho, J. H. Kim, S. H. Oh, H. H. Nam, J. M. Kim, J. H. Lee, *J. Biomed. Mater. Res., Part A* **2009**, *91A*, 400.
[29] A. S. Karakoti, O. Tsigkou, S. Yue, P. D. Lee, M. M. Stevens, J. R. Jones, S. Seal, *J. Mater. Chem.* **2010**, *20*, 8912.
[30] Y. Jin, S. Chen, J. Duan, G. Jia, J. Zhang, *J. Inorg. Biochem.* **2015**, *146*, 28.
[31] J. C. Zhang, S. J. Xu, K. Wang, S. F. Yu, *Chin. Sci. Bull.* **2003**, *48*, 2170.
[32] V. S. Shankar, A. S. M. T. Alam, C. M. R. Bax, B. E. Bax, M. Pazianas, C. L. H. Huang, M. Zaidi, *Biochem. Biophys. Res. Commun.* **1992**, *187*, 907.